Electronic Supplementary Information for

# Impact of Intermediate Sites on Bulk Diffusion Barriers: Mg Intercalation in $Mg_2Mo_3O_8$

Gopalakrishnan Sai Gautam[†,a,b,c], Xiaoqi Sun[†,d], Victor Duffort[d], Linda F. Nazar[*,d] and Gerbrand Ceder[*,b,c]

[†] - *Equal contributions*

[a]Department of Materials Science and Engineering, Massachusetts Institute of Technology, Cambridge, MA 02139, USA

[b]Materials Science Division, Lawrence Berkeley National Laboratory, Berkeley, CA 94720, USA

[c]Department of Materials Science and Engineering, University of California Berkeley, CA 94720, USA

[d]Department of Chemistry and the Waterloo Institute of Nanotechnology, University of Waterloo, ON N2L3G1, Canada

## Experimental methods

**Synthesis and characterization.** $Mg_2Mo_3O_8$ was synthesized by heating a 1:1 mixture of MgO and $MoO_2$ at 1000 ºC for 12 hours under Ar flow. The small amount of MgO impurity was washed away with 1M HCl. X-ray diffraction (XRD) was carried out on the PANalytical Empyrean using Cu Kα radiation with Bragg-Brentano geometry. De-magnesiation was carried out by stirring the pristine material in 0.2 M $NO_2BF_4$ (Sigma-Aldrich, 95%) in acetonitrile (Caledon, 99.9%, dried over 3 Å molecular sieves) at 1:4 molar ratio for 1 day in an Ar-filled

glovebox ($O_2$ and $H_2O$ level below 5 ppm). The product was filtered and washed with acetonitrile. The fraction of crystalline phase in the demagnesiated material was estimated by the external standard method. Typically, the demagnesiated product was ground with silicon (325 mesh, Sigma-Aldrich, 99%) in 9:1 weight ratio in Ar-filled glovebox and sealed in 0.3 mm glass capillary. XRD was carried out with the Debye-Scherrer geometry. Rietveld refinements[1] were performed with FullProf suite.[2] Refining Mg occupancies did result in any change from the pristine composition so they were fixed at 1. The refined $Mg_2Mo_3O_8$:Si weight ratio was 0.54:0.46 (**Table S1b**), resulting in 13 wt% of crystalline phase in the demagnesiated sample. The morphologies and elemental ratios of the materials were studied with a Zeiss field emission scanning electron microscope (SEM) equipped with an energy dispersive X-ray spectroscopy (EDX) detector.

**Electrochemistry.** For non-aqueous tests, positive electrodes were prepared by mixing the pristine material with super P and polyvinylidene fluoride (PVDF, Sigma-Aldrich, average Mw ~ 534,000) at 8:1:1 weight ratio in N-methyl-2-pyrrolidone (NMP, Sigma-Aldrich, 99.5%) and casting on Mo foil. APC electrolyte was synthesized with previous reported procedure.[3] Magnesium metal was polished with carbide paper (Mastercraft ®, 180 grit SiC), cleaned with Kimwipe and served as the counter and reference electrode. The 2325 coin cells with the positive electrode side protected by Mo foil were assembled in an Ar-filled

glovebox. In aqueous system, slurry with the same recipe was used and casted on Ti foil. The electrode was assembled in the T-shape Swagelok three-electrode cell with Pt gauze (Sigma-Aldrich, 99.9%) counter, Ag/AgCl reference electrode, and 0.5 M $Mg(ClO_4)_2$ in deionized water electrolyte. Galvanostatic tests were carried out on the Bio-logic VMP3 cycler.

**Computational methods**

**First-principles calculations.** Density Functional Theory (DFT), as implemented in the Vienna Ab-Initio Simulation Package (VASP),[4,5] with the Perdew – Burke – Ernzerhof (PBE)[6] exchange-correlation functional was used for all computations. A Γ-centered *k*-point mesh of 4 x 4 x 2 was used to sample wave functions, which were described by the Projector Augmented Wave (PAW)[7] theory and a well-converged energy cut-off of 520 meV. For the voltage calculations, a Hubbard *U* correction of 4.38 eV[8] was added to the Generalized Gradient Approximated (GGA) Hamiltonian to remove the spurious self-interaction errors of the molybdenum *d* electrons.[9] All structures were fully relaxed to within 0.01 meV/atom.

The migration barriers for Mg diffusion in the $Mg_2Mo_3O_8$ structure were calculated using the Nudged Elastic Band (NEB)[10] method as implemented in VASP. While a total of 7 images were used to capture the trajectory of $Mg^{2+}$ diffusion, the forces were converged within 50 meV/Å. Besides introducing a

minimum distance of ~ 9 Å between the diffusing atoms, standard GGA was used for the calculation of the migration barriers due to the problematic convergence of GGA+*U* NEB calculations, as previously noted in the literature.[11]

**Voltage calculations.** In order to compute the average voltage for Mg intercalation between the ranges of $1 \leq x_{Mg} \leq 2$ and $0 \leq x_{Mg} \leq 1$ in $Mg_xMo_3O_8$, the stable Mg-vacancy ordering at $x_{Mg} = 1$ needs to be determined. To do so, we considered four Mg-vacancy orderings, as displayed in **Figure S3**, enumerated in a conventional $Mo_3O_8$ cell, which consists of 16 oxygen atoms. Based on the calculated energies, the Mg-vacancy ordering where Mg solely occupies octahedral sites (**Figure S3a**) was found to be the most stable.

Once the stable Mg-ordering at $x_{Mg} = 1$ was determined, average voltages were calculated using the well known methodology of Aydinol *et al.*[12] Calculated average voltages are displayed in **Figure S4**, while there is good agreement between the open-circuit voltage observed in experiments (~ 2.5 V) and the theoretical voltage calculated for $1 \leq x_{Mg} \leq 2$ (~ 2.6 V, red curve in **Figure S4**).

**Table S1a.** Refined parameters for pristine $Mg_2Mo_3O_8$ (space group = $P6_3mc$, a = 5.76375(4) Å, c = 9.89549(8) Å, $\chi^2$ = 4.39, Bragg R-factor = 2.22)

| Atom | Wyck. | x | y | z | Occ. | $B_{iso}$ (Å$^2$) |
|---|---|---|---|---|---|---|
| Mo | 6c | 0.14639(4) | 0.85361(4) | 0.250(5) | 1 | 0.050(4) |
| Mg1 | 2b | 0.33333 | 0.66667 | 0.948(5) | 1 | 0.43(4) |
| Mg2 | 2b | 0.33333 | 0.66667 | 0.513(5) | 1 | 0.43(4) |
| O1 | 2a | 0 | 0 | 0.397(5) | 1 | 0.13(3) |
| O2 | 2b | 0.33333 | 0.66667 | 0.142(5) | 1 | 0.13(3) |
| O3 | 6c | 0.4881(4) | 0.5119(4) | 0.371(5) | 1 | 0.13(3) |
| O4 | 6c | 0.1682(6) | 0.8318(6) | 0.632(5) | 1 | 0.13(3) |

**Table S1b.** Refined parameters for a mixture of 90 wt% fully demagnesiated $Mg_2Mo_3O_8$ and 10 wt% silicon standard ( $\chi^2$ = 4.99)

| Atom | Wyck. | x | y | z | Occ. | $B_{iso}$ (Å$^2$) |
|---|---|---|---|---|---|---|
| **$Mg_2Mo_3O_8$, S.G. = $P6_3mc$, a = 5.76446(6) Å, c = 9.8969(2) Å, 54.0(6) wt%, Bragg R-factor = 4.27** | | | | | | |
| Mo | 6c | 0.14632(8) | 0.85368(8) | 0.250(6) | 1 | 0.071(6) |
| Mg1 | 2b | 0.33333 | 0.66667 | 0.949(6) | 1 | 0.50(6) |
| Mg2 | 2b | 0.33333 | 0.66667 | 0.513(6) | 1 | 0.50(6) |
| O1 | 2a | 0 | 0 | 0.397(6) | 1 | 0.21(4) |
| O2 | 2b | 0.33333 | 0.66667 | 0.143(6) | 1 | 0.21(4) |
| O3 | 6c | 0.4880(9) | 0.51204(9) | 0.371(6) | 1 | 0.21(4) |
| O4 | 6c | 0.172(1) | 0.828(1) | 0.632(6) | 1 | 0.21(4) |
| **Silicon, S.G. = Fd-3m, a = 5.43175(6) Å, 46.0(6) wt%, Bragg R-factor = 4.02** | | | | | | |
| Si | 8a | 0.875 | 0.875 | 0.875 | 1 | 0.527(6) |

**Table S1c.** Refined parameters for partially demagnesiated $Mg_2Mo_3O_8$ (space group = $P6_3mc$, a = 5.76384(9) Å, c = 9.8960(2) Å, $\chi^2$ = 4.82, Bragg R-factor = 3.65)

| Atom | Wyck. | x | y | z | Occ. | $B_{iso}$ (Å$^2$) |
|---|---|---|---|---|---|---|
| Mo | 6c | 0.14626(5) | 0.85374(5) | 0.250(8) | 1 | 0.059(4) |
| Mg1 | 2b | 0.33333 | 0.66667 | 0.950(8) | 1 | 0.42(4) |
| Mg2 | 2b | 0.33333 | 0.66667 | 0.512(8) | 1 | 0.42(4) |
| O1 | 2a | 0 | 0 | 0.396(8) | 1 | 0.27(3) |
| O2 | 2b | 0.33333 | 0.66667 | 0.146(8) | 1 | 0.27(3) |
| O3 | 6c | 0.4886(6) | 0.5114(6) | 0.369(8) | 1 | 0.27(3) |
| O4 | 6c | 0.1747(8) | 0.8253(8) | 0.633(8) | 1 | 0.27(3) |

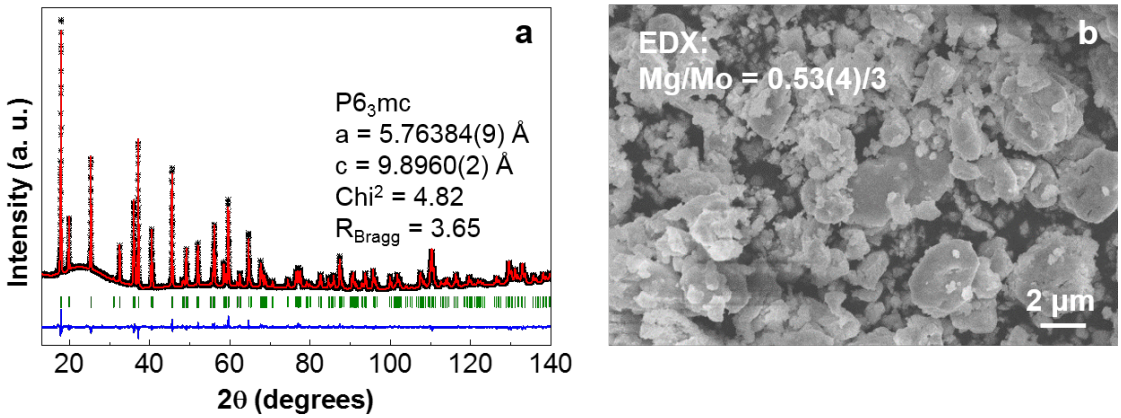


**Figure S1.** (a) Rietveld refinement fit of partially demagnesiated $Mg_2Mo_3O_8$ ($Mg_2Mo_3O_8$:$NO_2BF_4$ = 1:2). Black crosses – experimental data, red lines – fitted data, blue line – difference map between observed and calculated data, green ticks – the $P6_3mc$ phase. (b) SEM image and EDX result.

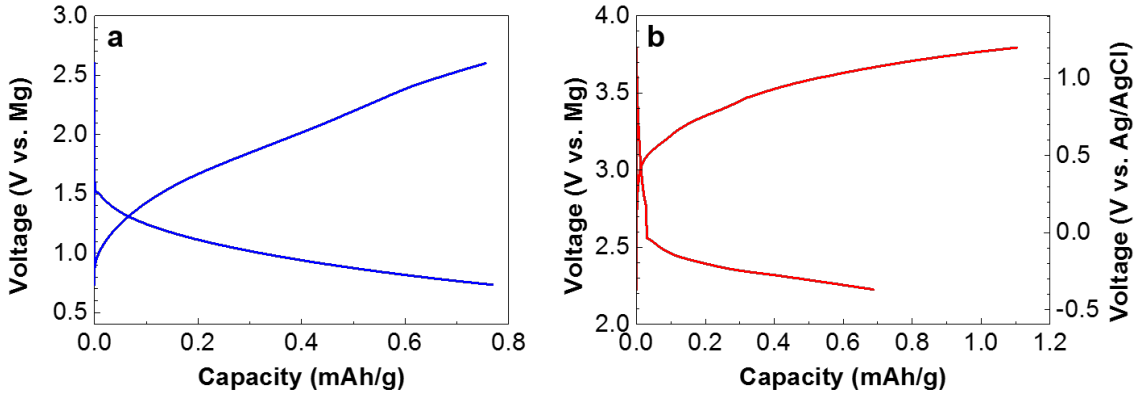


**Figure S2.** Electrochemistry of $Mg_2Mo_3O_8$ tested in (a) 0.4M APC and (b) 0.5M $Mg(ClO_4)_2$ in water at C/20 (1Mg/$Mg_2Mo_3O_8$ in 20 hours) rate and room temperature, showing no activity.

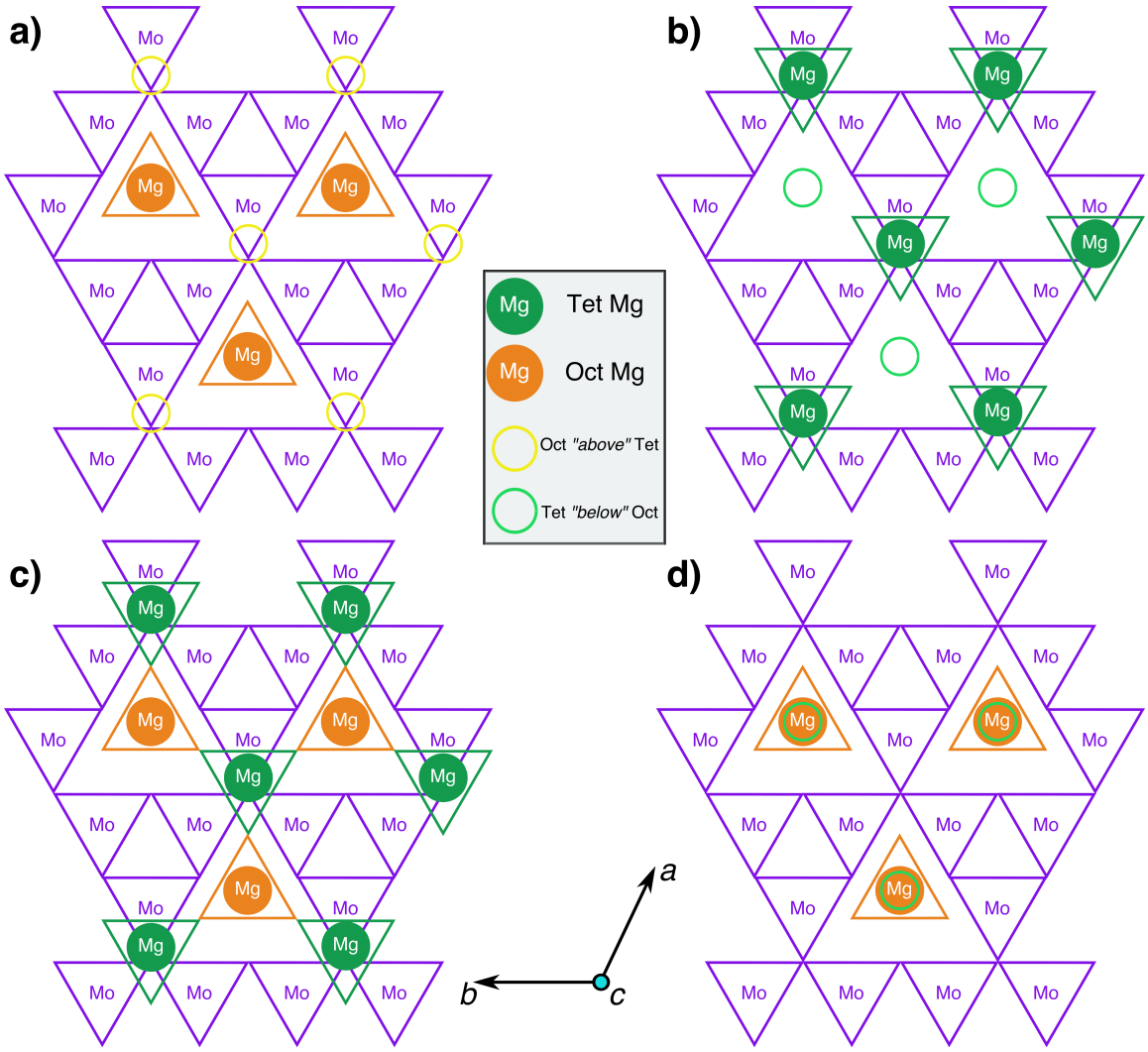


**Figure S3.** 2D view of the Mg-vacancy ordering enumerated for evaluating the stable Mg configuration at $x_{Mg}$ = 1. While (a) and (b) have Mg occupancy solely of octahedral (orange, yellow circles) and tetrahedral (green circles) sites, (c) and (d) correspond to an equal Mg distribution among tetrahedral and octahedral sites. All the configurations are viewed along the layer spacing direction (*c*-axis).

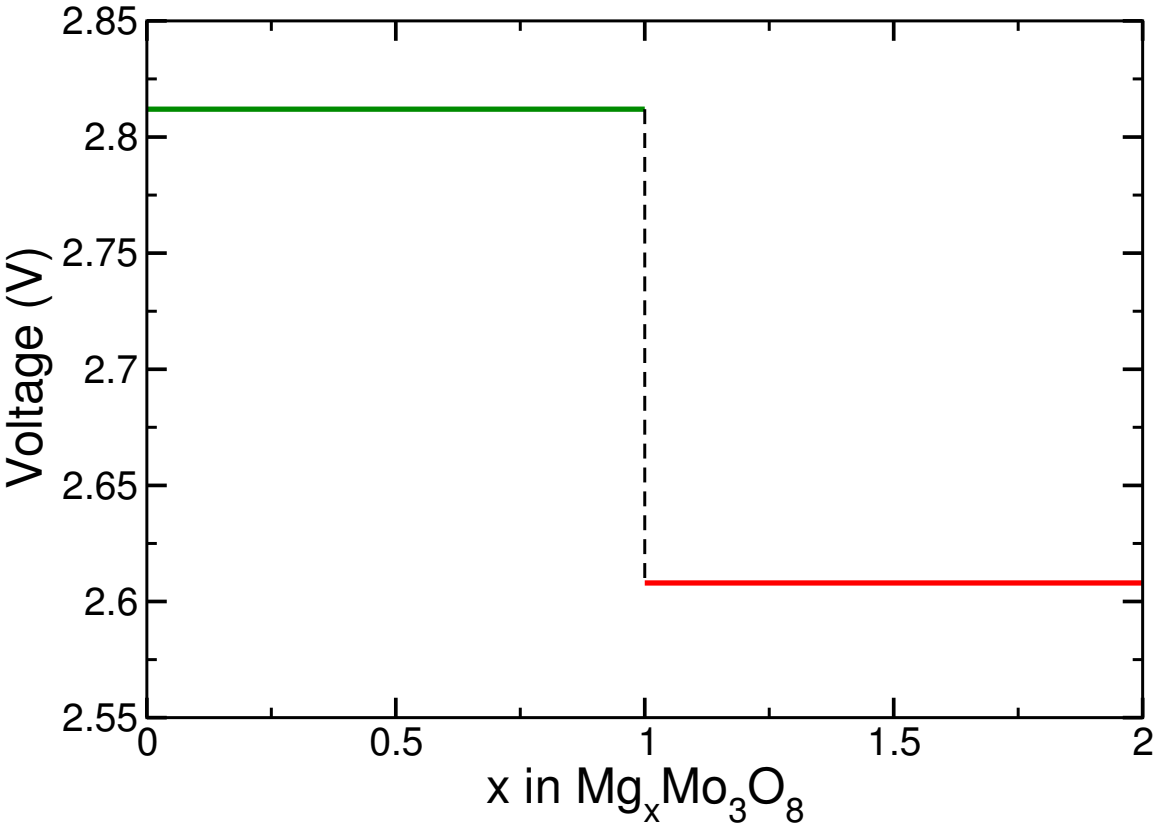


**Figure S4.** Average voltage for Mg intercalation, as calculated for the $1 \leq x_{Mg} \leq 2$ (red) and $0 \leq x_{Mg} \leq 1$ (green) concentration ranges.

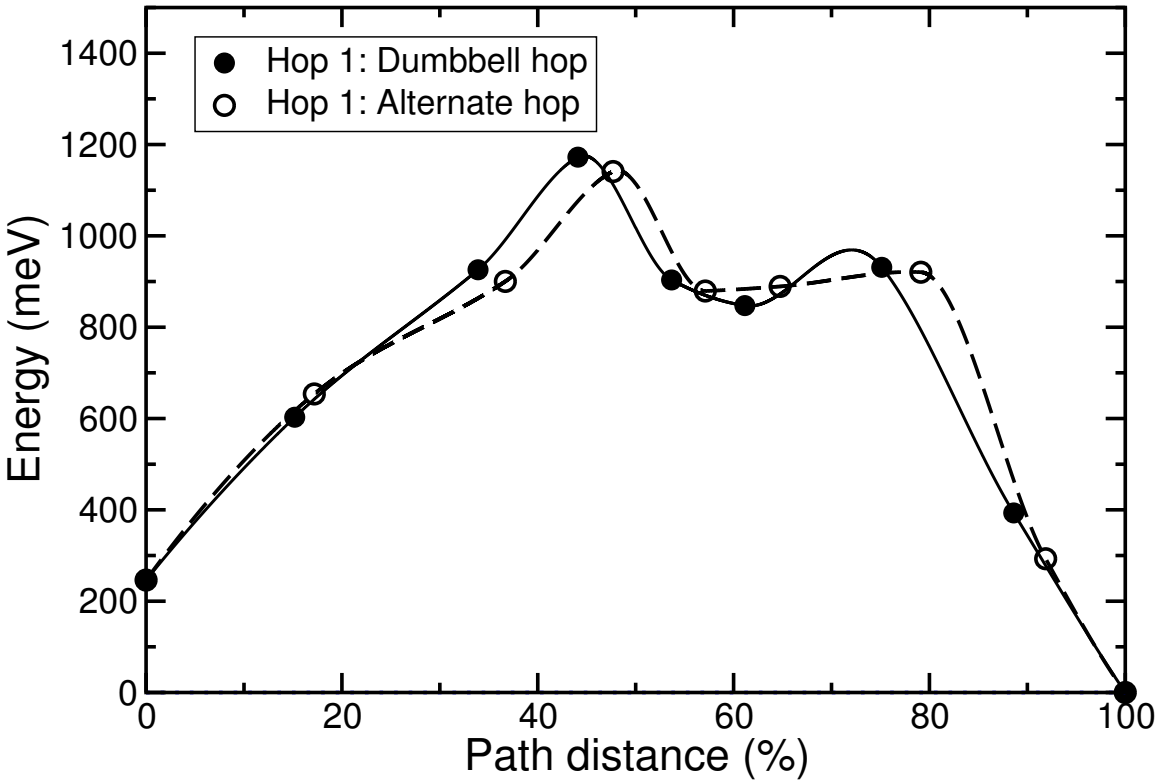


**Figure S5.** The migration barriers for Hop 1 along the O—Mg—O dumbbell path (solid line, identical to **Figure 4a** in the main text) and the barrier for the alternate hop as illustrated in **Figure 4c** (dashed lines). Although the alternate pathway for hop 1 was initialized with intermediate tetrahedral and octahedral sites, the NEB calculations converged to a pathway similar to the O—Mg—O dumbbell path, with a similar barrier magnitude.

## References


(1) Rietveld, H. M. A Profile Refinement Method for Nuclear and Magnetic Structures. *J. Appl. Cryst.* **1969**, *2*, 65-71.

(2) Rodríguez-Carvajal, J. Recent Advances in Magnetic Structure Determination by Neutron Powder Diffraction. *Physica B*, **1993**, *192*, 55-69.

(3) Mizrahi, O.; Amir, N.; Pollak, E.; Chusid, O.; Marks, V.; Gottlieb, H.; Larush, L.; Zinigrad E.; Aurbach, D. Electrolyte Solutions with a Wide Electrochemical Window for Rechargeable Magnesium Batteries. *J. Electrochem. Soc.*, **2008**, *155*, A103-A109.

(4) Kresse G.; Hafner, J. Ab initio molecular dynamics for liquid metals. *Phys. Rev. B* **1993**, *47*, 558-561.

(5) Kresse, G.; Furthmüller, J. Efficient iterative schemes for ab initio total-energy calculations using a plane-waves basis set. *Phys. Rev. B* **1996**, *54*, 11169-11186.

(6) Perdew J. P.; Burke, K.; Ernzerhof, M. Generalized Gradient Approximation made simple. *Phys. Rev. Lett.* **1996**, *77*, 3865-3868.

(7) Kresse, G.; Joubert, D. From ultrasoft pseudopotentials to the projector augmented-wave method. *Phys. Rev. B.* **1999**, *59*, 1758-1775.

(8) Jain, A.; Hautier G.; Ong, S. P.; Moore, C. J.; Fischer, C. C.; Persson, K. A.; Ceder, G. Formation enthalpies by mixing GGA and GGA + U calculations. *Phys. Rev. B* **2011**, *84*, 045115.

(9) Anisimov, V. I.; Zannen, J.; Andersen, O. K. Band theory and Mott insulators: Hubbard U instead of Stoner I. *Phys. Rev. B* **1991**, *44*, 943-954.

(10) Sheppard, D.; Terrell, R.; Henkelman, G. Optimization methods for finding minimum energy paths. *J. Chem. Phys.* **2008**, *128*, 134106.

(11) Liu, M.; Rong, Z.; Malik, R.; Canepa, P.; Jain, A.; Ceder, G.; Persson, K. A. Spinel compounds as multivalent battery cathodes: A systematic evalulation based on ab initio calculations. *Energy Environ. Sci.* **2015**, *8*, 964-974.

(12) Aydinol, M. K.; Kohan, A.; Ceder, G. Ab initio calculation of the intercalation voltage of lithium-transition-metal oxide electrodes for rechargeable batteries. *J. Power Sources* **1997**, *68*, 664-668.